Systematic Study of Quasifission in ^{48}Ca-induced reactions

B. M. A. Swinton-Bland[1,*], D. J. Hinde[1], M. Dasgupta[1], D. Y. Jeung[1], E. Williams[1], K. J. Cook[1,**], E. Prasad[1,***], D. C. Rafferty[1], C. Sengupta[1], C. Simenel[1], E. C. Simpson[1], J. F. Smith[1,****], K. Vo-Phuoc[1], and J. Walshe[1]

[1]Department of Nuclear Physics, Research School of Physics, The Australian National University, Canberra, ACT 2601, Australia.

Abstract. The production of superheavy elements through the fusion of two heavy nuclei is severely hindered by the quasifission process, which results in the fission of heavy systems before an equilibrated compound nucleus (CN) can be formed. The heaviest elements have been synthesised using ^{48}Ca as the projectile nucleus. However, the use of ^{48}Ca in the formation of new superheavy elements has been exhausted, thus a detailed understanding of the properties that made ^{48}Ca so successful is required. Measurements of mass-angle distributions allow fission fragment mass distribution widths to be determined. The effect of the orientation of prolate deformed target nuclei is presented. Closed shells in the entrance channel are also shown to be more important than the stability of the formed CN in reducing the quasifission component, with reduced mass widths for reactions with the closed shell target nuclei ^{144}Sm and ^{208}Pb. Comparison to mass widths for ^{48}Ti-induced reactions show a significant increase in the mass width compared to ^{48}Ca-induced reactions, highlighting the difficulty faced in forming new superheavy elements using projectiles with higher atomic number than ^{48}Ca.

1 Introduction

Superheavy elements (SHEs) mark the upper boundary of the existence of atomic nuclei. Their production offers an insight into exotic nuclear structure, and provides thorough tests of established nuclear models. Oganesson ($^{294}_{118}$Og) represents the heaviest element synthesised to date, produced in the ^{48}Ca + ^{249}Cf reaction [1, 2]. For a SHE to be produced, two heavy nuclei must come into contact and form an equilibrated compound nucleus (CN), by evolving from the di-nuclear shape at contact, to that of a compact system [3, 4]. Due to the large repulsive Coulomb force, the system often instead breaks apart before this equilibrated system is reached. This process is known as quasifission (QF) [5–7]. This significantly suppresses the yield of desired products, and can be the most significant hindrance to SHE formation.

The difficulty in forming SHEs is further compounded by the need for heavier projectile nuclei than ^{48}Ca, as production of targets of elements heavier than Cf is currently not achievable. ^{48}Ca has been successfully used in SHE formation reactions, due in part to its high N/Z ratio and doubly magic shell structure [8, 9]. However, to form elements 119 or larger, heavier projectiles must be used, which should have similar properties to ^{48}Ca. The most favourable projectiles are expected to be ^{50}Ti and ^{54}Cr, however neither of these are doubly magic, nor as neutron-rich as ^{48}Ca [9]. A recent study [10] highlighted that the lack of these key characteristics of ^{48}Ca in both ^{50}Ti and ^{54}Cr leads to a significant reduction in the probability of forming an equilibrated CN.

There has been a surge in experimental and theoretical investigations of quasifission in recent years. The complex dynamics has many different dependencies, with experiments highlighting the influence of entrance channel properties such as nuclear deformation and orientation [11–16], mass asymmetry [3, 5, 17, 18], magicity [19, 20] and shell structure [21–24]. The multiple parameters that have significant effects on fusion cross sections serve to highlight the complexity of the dynamics, and the challenge that is posed to produce a model that can account for all of these effects.

A systematic study of ^{48}Ca-induced reactions with a variety of target nuclei at energies close to the Coulomb barrier is presented. Mass-angle distributions (MADs) were measured, and fission fragment mass distribution widths were determined. The targets used in this work range from the spherical ^{144}Sm, to strongly deformed nuclei, such as ^{170}Er and ^{186}W, through to the spherical ^{208}Pb. These targets allow the investigation of the role of deformation in this work. Moreover, the role of closed shells is demonstrated due to the fact that the ^{48}Ca projectile and ^{208}Pb target both have full proton and neutron shells, whilst ^{144}Sm has a closed neutron shell.

2 Mass-Angle Distributions and Mass Widths

MADs show the distribution of fission fragment masses as a function of centre-of-mass scattering angle, $\theta_{\mathrm{c.m.}}$. This

*e-mail: ben.swinton-bland@anu.edu.au
**Present Address: National Superconducting Cyclotron Laboratory, Michigan State University, East Lansing, MI 48824, USA
***Present address: Department of Physics, Central University of Kerala, Kasaragod 671316, India
****Present address: Advanced Technology Institute, University of Surrey, Guildford, Surrey GU2 7XH, United Kingdom.

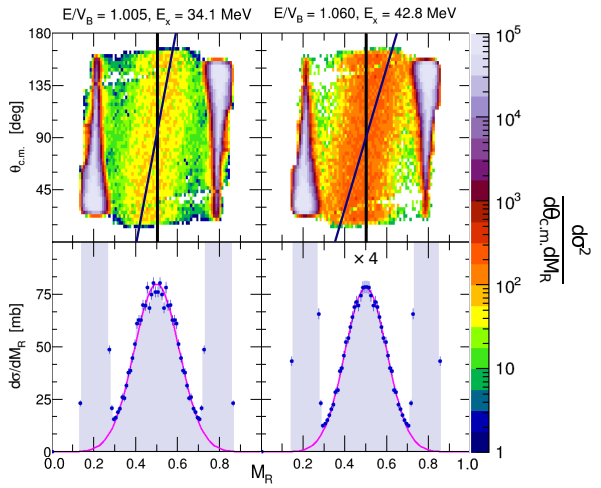

Figure 1. MAD scatter plots (top row) and projections onto the M_R axis (bottom row) for the ^{48}Ca + ^{186}W reaction at two different energies. The centre-of-mass energies with respect to the Coulomb barrier, E/V_B, and the excitation energies, E_x, are shown at the top of each plot. The intensity scale represents the double differential cross section, $d\sigma^2/d\theta_{c.m.}dM_R$ in mb/rad, per pixel. The multiplicative factor scales the y-axis that is shown for the M_R distributions for each plot. The blue lines highlight the strong mass-angle correlation present in this reaction.

offers an additional method to characterise QF in a model-independent way [5, 6, 25]. MADs offer the most direct evidence of QF, which appears as a correlation between the fission fragment mass with scattering angle. MADs not only allow QF to be measured, but also the fusion-fission (FF) process, whereby the formed CN undergoes fission. FF primarily results in mass-symmetric fission fragments.

Importantly, as all degrees of freedom must be equilibrated, FF results in a narrow fission mass distribution. QF, however, will have a much broader mass distribution than FF. This arises due to the mass degree of freedom failing to achieve complete relaxation as the system re-separates before the formation of an equilibrated CN. Therefore, by comparing the determined mass distribution widths, given by the standard deviation of a Gaussian fit to the mass distributions, the amount of QF in a given reaction can be estimated, and has been used extensively [21, 26–28].

At the Australian National University, a wide ranging program measuring MADs is taking place. To measure experimental MADs for the reactions of interest, pulsed beams of ^{48}Ca with ∼1 ns width and 106.9 ns separation were produced at the Heavy Ion Accelerator Facility at the Australian National University using the 14UD tandem accelerator. Beams were bombarded onto isotopically enriched targets of ^{144}Sm, ^{170}Er, ^{176}Yb, ^{180}Hf, ^{186}W, ^{192}Os, ^{198}Pt, ^{204}Hg, and ^{208}Pb. The subsequent fission fragments were detected using the ANU CUBE detector system [12, 29], which is composed of two large-area, position sensitive Multi-Wire Proportional Counters (MWPCs) and one MWPC approximately half the size, which was situated at extreme backward angles to provide a wider angular coverage. The position and timing information from the MWPCs were used to obtain fragment velocities and centre-of-mass angles. The velocities are then used to determine the binary mass-splits, characterised by the mass ratio, $M_R = M_1/(M_1 + M_2)$, where $M_{1,2}$ are the masses of the two measured fragments. Thus, MADs for all reactions studied could be produced, with example MADs and mass distributions for the ^{48}Ca + ^{186}W reaction shown in Fig. 1. The strong correlation of fragment mass with angle is a clear indication of a strong QF component in this reaction. This correlation also presents itself as a wide mass distribution width, seen in the bottom panels of Fig. 1.

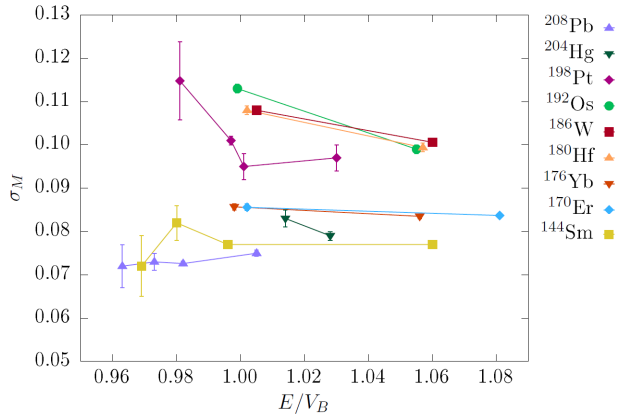

Figure 2. The measured mass widths, σ_M, presented as a function of the centre-of-mass energy with respect to the capture barrier for all reactions measured in this work. The error bars are determined from the calculated uncertainty in the standard deviations of the Gaussian fits for each reaction. The lines are used to guide the eye between each data point to highlight the general trends for each reaction. The two spherical targets, ^{144}Sm and ^{208}Pb, show a significantly different trend to the all other targets, with an increase in σ_M with increasing energy being observed.

3 Orientation and Deformation Effects

The measured mass widths, represented by the standard deviations of the Gaussian fits to the mass distributions, for all reactions studied as a function of the centre-of-mass energy with respect to the capture barrier, E/V_B, are plotted in Fig. 2. The error bars represent the calculated uncertainty in the mass widths, determined from the uncertainty in the standard deviations of the Gaussian fits to the mass distributions. Lines connecting each point guide the eye. Firstly, the spherical target nuclei, ^{144}Sm and ^{208}Pb, show a markedly different trend to the deformed target nuclei. There is a slight increase in the mass width with E/V_B for the spherical nuclei, whilst the mass widths for the deformed nuclei decrease as E/V_B increases. These trends can be attributed to the dependence on the orientations of the deformed target nuclei with reaction energy.

The reduction of mass width with increasing energy for the deformed nuclei is expected, as there is an increasing probability of reactions where the deformation axes of the deformed targets are anti-aligned with the projectile nucleus [12]. For the anti-aligned orientation the dinuclear shape is far more compact than the aligned case, which is the only accessible orientation at below barrier

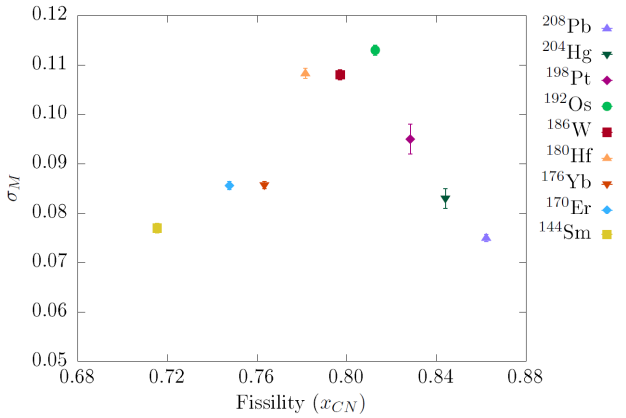

Figure 3. The measured mass widths, σ_M, presented as a function of the compound nucleus fissility, x_{CN}, for reactions at $E/V_B = 1.0 \pm 0.1$. The error bars are determined from the calculated errors in the standard distributions of the Gaussian fits for each reaction. The decrease in σ_M between the ^{192}Os and ^{208}Pb reactions highlights that the entrance channel magicity dominates the effect of an increased fissility of the CN.

energies. Thus, the anti-aligned orientation has a significantly reduced inertial force acting upon it which significantly increases the probability of forming a CN. For the spherical nuclei, there is only one available orientation. An increased beam energy will produce a CN with a higher excitation energy, therefore resulting in an increased mass width. This is due to the increased thermal fluctuations in the mass-splits introduced with a higher excitation energy, which broadens the mass distribution. An increased beam energy also results in an increased angular momentum, further increasing the probability of QF, which may contribute to a broader mass width.

Overall, the general trends in the determined mass widths as a function of E/V_B highlight the importance of the available reaction outcomes on the alignment of the statically deformed target nuclei with increasing energy. This orientation dependence is also crucial in new SHE formation reactions, as the heaviest elements ($Z \geq 113$) have been produced through hot fusion reactions with actinide targets which all have substantial deformations [8, 30].

4 Effect of Magicity and Fissility

The influence of closed shells in the exit channel can also be investigated using the determined mass widths of all reactions at a particular reaction energy. By plotting the mass widths as a function of the CN fissility parameter, x_{CN}, as in Fig. 3, the balance between the entrance and exit channel nuclear structure can be investigated.

The CN fissility is a measure of the inherent instability of the formed CN, which represents the balance between the repulsive Coulomb force and the strong attractive nuclear force. From the formalism of Ref. [31], the fissility is given by:

$$x_{\mathrm{CN}} = \frac{(Z^2/A)}{(Z^2/A)_{\mathrm{crit}}}, \qquad (1)$$

where Z and A are the proton and total nucleon numbers of the CN, respectively. The $(Z^2/A)_{\mathrm{crit}}$ is given by:

$$(Z^2/A)_{\mathrm{crit}} = 50.883(1 - 1.7826I^2), \qquad (2)$$

where $I = (A - 2Z)/A$ is the relative neutron excess of the CN.

Most reactions have a determined mass width at an energy very close to $E/V_B = 1.0$, except ^{204}Hg, whose closest data point is at $E/V_B = 1.014$. This is still reasonably close and so is included in Fig. 3 for completeness.

Firstly, one would expect a monotonic increase of σ_M with fissility in the absence of nuclear structure effects. However, what is observed in Fig. 3 is instead a significant increase in σ_M with fissility up to ^{192}Os, followed by a rapid decrease. This immediately indicates that the shell effects in the entrance channel are far more significant than the fissility of the CN. The decrease strongly correlates with the decrease in static deformation from ^{192}Os to ^{208}Pb. Furthermore, the presence of closed shells in the entrance channel may also contribute to the decrease in mass width [32]. The two targets that have magic shells, ^{144}Sm and ^{208}Pb, have the smallest σ_M values. The largest σ_M values correspond to the targets that lie the furthest from shell closures, ^{180}Hf, ^{186}W, and ^{192}Os.

5 Comparison to ^{48}Ti-induced reactions

The importance of magicity in the entrance channel is also apparent when comparing the mass widths for the doubly magic ^{48}Ca-induced reactions measured here with those measured for ^{48}Ti-induced reactions by Lin *et al.* [13]. The ^{48}Ti-induced reactions were measured for targets either identical or very similar to those measured in this study, at similar E/V_B values, allowing for direct comparison between a doubly magic projectile and a non-magic projectile.

By comparing the mass widths from the ^{48}Ti-induced and ^{48}Ca-induced reactions on the same target nucleus at $E/V_B = 1.00 \pm 0.01$, the amount of QF present in both reactions can be directly compared. Overall, the mass widths range from $\sim 20\%$ to $\sim 110\%$ larger for the ^{48}Ti-induced reactions. This highlights that there is considerably more QF in reactions with the non-magic ^{48}Ti compared with the doubly magic ^{48}Ca projectile. The increase in QF can also be attributed to the increased proton number of Ti compared to Ca [29].

6 Conclusions

Overall, the general trends in the mass distributions across all reactions indicate that there are many different variables that severely affect the QF process. The role of a variety of nuclear structure effects, for reactions close to the Coulomb barrier, have a considerable effect on the observed reaction dynamics. Deformation has been shown to determine the possible reactions that can take place, whilst magicity in the entrance channel suppresses the presence of QF. The comparisons between the measured mass widths of ^{48}Ti and ^{48}Ca highlight that the use of a

heavier projectile, with no magicity, severely reduces the likelihood of forming a CN. This emphasises the difficulty faced in synthesising element 119 and beyond.

Acknowledgements

The authors acknowledge NCRIS operations support for the ANU Heavy Ion Accelerator Facility. We also acknowledge the Australian Research Council for support through Discovery grants DP160101254, DP170102318, and DP170102423.

References

[1] Y. T. Oganessian, V. K. Utyonkov, Y. V. Lobanov *et al.*, Phys. Rev. C **74**, 044602 (2006).
[2] Y. T. Oganessian, J. Phys. G Nucl. Partic. **34**, R165 (2007).
[3] R. Rafiei, R. G. Thomas, D. J. Hinde *et al.*, Phys. Rev. C **77**, 024606 (2008).
[4] A. Diaz-Torres, G. Adamian, N. Antonenko *et al.*, Phys. Rev. C **64**, 024604 (2001).
[5] J. Tōke, R. Bock, G. Dai *et al.*, Nucl. Phys. A **440**, 327 (1985).
[6] W. Q. Shen, J. Albinski, A. Gobbi *et al.*, Phys. Rev. C **36**, 115 (1987).
[7] B. B. Back, R. R. Betts, J. E. Gindler *et al.*, Phys. Rev. C **32**, 195 (1985).
[8] Y. T. Oganessian, F. S. Abdullin, P. D. Bailey *et al.*, Phys. Rev. Lett. **104**, 142502 (2010).
[9] Y. T. Oganessian, V. K. Utyonkov, Nucl. Phys. A **944**, 62 (2015).
[10] K. Banerjee, D. J. Hinde, M. Dasgupta *et al.*, Phys. Rev. Lett. **122**, 232503 (2019).
[11] D. J. Hinde, M. Dasgupta, J. R. Leigh *et al.*, Phys. Rev. Lett. **74**, 1295 (1995).
[12] D. J. Hinde, M. Dasgupta, J. R. Leigh *et al.*, Phys. Rev. C **53**, 1290 (1996).
[13] C. J. Lin, R. du Rietz, D. J. Hinde *et al.*, Phys. Rev. C **85**, 014611 (2012).
[14] K. Nishio, H. Ikezoe, S. Mitsuoka *et al.*, Phys. Rev. C **63**, 044610 (2001).
[15] K. Nishio, H. Ikezoe, S. Mitsuoka *et al.*, Phys. Rev. C **77**, 064607 (2008).
[16] J. C. Mein, D. J. Hinde, M. Dasgupta *et al.*, Phys. Rev. C **55**, R995 (1997).
[17] A. C. Berriman, D. J. Hinde, M. Dasgupta *et al.*, Nature **413**, 144 (2001).
[18] B. B. Back, P. B. Fernandez, B. G. Glagola *et al.*, Phys. Rev. C **53**, 1734 (1996).
[19] C. Simenel, D. J. Hinde, R. du Rietz *et al.*, Phys. Lett. B **710**, 607 (2012).
[20] M. G. Itkis, A. A. Bogachev, I. M. Itkis *et al.*, Nucl. Phys. A **787**, 150 (2007).
[21] A. Wakhle, C. Simenel, D. J. Hinde *et al.*, Phys. Rev. Lett. **113**, 182502 (2014).
[22] A. Diaz-Torres, Phys. Rev. C **74**, 064601 (2006).
[23] M. G. Itkis, S. Beghini, A. A. Bogachev *et al.*, Nucl. Phys. A **734**, 136 (2004).
[24] E. M. Kozulin, G. N. Knyazheva, S. N. Dmitriev *et al.*, Phys. Rev. C **89**, 014614 (2014).
[25] R. Bock, Y. Chu, M. Dakowski *et al.*, Nucl. Phys. A **388**, 334 (1982).
[26] E. Williams, D. J. Hinde, M. Dasgupta *et al.*, Phys. Rev. C **88**, 034611 (2013).
[27] K. Hammerton, Z. Kohley, D. J. Hinde *et al.*, Phys. Rev. C **91**, 041602 (2015).
[28] D. J. Hinde, R. G. Thomas, R. du Rietz *et al.*, Phys. Rev. Lett. **100**, 202701 (2008).
[29] R. du Rietz, E. Williams, D. J. Hinde *et al.*, Phys. Rev. C **88**, 054618 (2013).
[30] Y. T. Oganessian, F. S. Abdullin, C. Alexander *et al.*, Phys. Rev. Lett. **109**, 162501 (2012).
[31] J. P. Blocki, H. Feldmeier, W. J. Swiatecki, Nucl. Phys. A **459**, 145 (1986).
[32] C. Simenel, D. J. Hinde, R. du Rietz *et al.*, Phys. Lett. B **710**, 607 (2012).